The Effect of Fluorination: A Crystallographic and Computational Study of Mesogenic Alkyl 4-[2-(Perfluorooctyl)ethoxy]benzoates

Megumi Yano,[b] Tetsuya Taketsugu,[b] Kayako Hori,*[a] Hiroaki Okamoto,[c] and Shunsuke Takenaka[c]

Abstract: The series of alkyl 4-[2-(per-fluorooctyl)ethoxy]benzoates (**F8-n**) shows a systematic change of crystal structures depending on the length of the alkyl chain: separate packing of perfluorooctyl (R_f) and alkyl (R_h) chains from each other for shorter ($n=$ 2) and longer ($n=11$) members, alternate packing of R_f and R_h chains for middle ($n=6,7$) members, and an intermediate type of packing for $n=4$. Semiempirical MO calculations show slightly repulsive interactions between the R_f chains, and attractive ones between R_f and R_h chains and between R_h and the core of a molecular pair. It is concluded that fluorination determines the molecular shape of the crystal structures by making the chain rigid. It is confirmed that the interactions between R_f chains are small compared with those between other moieties and that they are forced to aggregate owing to the exclusion from other moieties. Thus, the effect is dependent on the geometries and intermolecular interactions of the other moieties.

Keywords: intermolecular interaction · liquid crystals · perfluoroalkyl chains · semiempirical calculations · structure elucidation

Introduction

Various kinds of fluorinated compounds have been synthesized in order to produce, enhance, and modify the functions of materials, such as fluorous biphasic catalysts,[1] organic thin-film transistors,[2,3] and liquid crystals.[4] Fluorination has a significant effect on the properties of liquid crystalline compounds, such as their thermal stability and viscosity, as well as on the nature of the liquid crystal phase. It is well known that the introduction of fluorine atoms into a side chain enhances the smectic character of a liquid crystal.[5,6] The smectic A (S_A) phase is stabilized even for compounds with a core that consists of a single benzene unit owing to the stiffness of perfluoroalkyl (R_f) chains.[7–10] On the other hand, various liquid crystalline phases have been produced by the introduction of R_f chains. Lateral substitution of R_f chains into the cores produces columnar and/or a new type of lamellar structure in which the molecular axes are parallel to the layers.[11] Tetrahedral molecules of pentaerythritol derivatives also show enhanced liquid crystallinity, producing lamellar, columnar and/or cubic phases.[12] Furthermore, it has been revealed that fluorination is a very powerful and efficient strategy with which to construct self-assembled architectures that produce highly functional liquid crystals.[13–15] The strong ability of fluorinated molecules to produce supramolecular systems in dilute aqueous dispersions in contrast to their hydrocarbon counterparts has also been recognized.[16]

These significant results have been attributed to the micro-segregation of fluorinated and hydrocarbon moieties that is induced by different chemical properties.[17–20] Molecules with different chemical fragments are sometimes called polyphilic molecules.[21] It has been concluded from properties such as the low boiling points and low surface tensions of perfluorocarbons relative to the corresponding hydrocarbons that weak interactions exist between fluorinated moieties.[22] Thus, the effect of fluorination is called the "fluorophobic" effect. However, the term "fluorophilic" has also been used to describe the aggregation and/or affinity of fluorinated moieties.[16a,23,24] The crystal structures of several fluorinated compounds have been determined in order to elucidate the effect of fluorination. The remarkable stability of fluorine-substituted naphthalenebisimide has been attributed to the dense packing of R_f chains in the crystal, which prevents the penetration of oxygen and water.[2c] 4-Cyanophenyl 4-perfluoroheptylbenzoate crystallizes in a bilayer

[a] Prof. Dr. K. Hori
Department of Chemistry, Ochanomizu University
Bunkyo-ku, Tokyo 112-8610 (Japan)
Fax: (+81)3-5978-5335
E-mail: khori@cc.ocha.ac.jp

[b] M. Yano, Prof. Dr. T. Taketsugu
Graduate School of Humanities and Sciences
Ochanomizu University, Bunkyo-ku
Tokyo 112-8610 (Japan)

[c] Dr. H. Okamoto, Prof. Dr. S. Takenaka
Department of Advanced Materials Science and Engineering
Yamaguchi University, Ube 755-8611 (Japan)

structure due to strong CN—CN interactions,[25] while 4-per-fluoropropylmethoxyphenyl 4-undecyloxybenzoate has a monolayer stacking in which molecules are aligned in the same direction.[26] In the crystal of a chiral mesogen with a perfluoroheptylethoxy group, molecules are arranged in a head-to-tail fashion with two of four independent molecules oriented in the same direction and the other two in the opposite direction.[27] In our recent work, ethyl 4-[2-(perfluoro-octyl)ethoxy]benzoate and 2-[2-(perfluorooctyl)ethoxy]nitrobenzene have similar packing modes in which R_f chains aggregate in bilayer structures despite the different substituents.[28]

In order to understand and evaluate the effect of fluorination from a fundamental aspect, systematic crystal structure analysis has been carried out together with the computational evaluation of rather simple compounds. The homologous series of the ethyl compound mentioned above, alkyl 4-[2-(perfluorooctyl)ethoxy]benzoates (**F8-n**), has a simple mo-

$$C_8F_{17}C_2H_4O \quad \text{—} \quad \text{—} \quad COOC_nH_{2n+1}$$
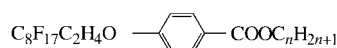
lecular constitution of an R_f chain, an alkyl (R_h) chain, and a core moiety comprising only a single aromatic ring. The S_A phase, although monotropic, appears in shorter ($n \leq 5$)[9a] and longer members ($n \geq 11$) but not in middle members of the series, as shown in Figure 1.[9b]

This behavior is unique as compounds with chains of intermediate length usually favor liquid crystalline phases. Comparison of the members of the series with and without the S_A phase should give us a better understanding of the effect. This paper describes the crystal structures of **F8-4**, **F8-6**, **F8-7**, and **F8-11**, and compares them with that of **F8-2**.[28] The results of energy partitions of intermolecular interactions between four nearest-neighbor molecules calculated by using the MOPAC2000 software package[29] are also described.

Figure 1. Transition temperatures for the **F8-n** series. Crystal-isotropic transitions (●) and S_A-isotropic transitions on cooling (■). Adapted from reference [9b].

Several carbon atoms in the chains have large and elongated temperature ellipsoids. Several C—C bonds in the R_f chains, especially in the highly disordered C molecule, have shorter bond lengths and wider angles than normal. In addition, several peaks of up to 2 e Å⁻³ remained around the R_f chains. All these results suggest that in the highly disordered chains, librational and/or flip-flop motions of the zigzag C-C-C skeleton are quenched at low temperatures. The fluorine atoms in **F8-11** are also highly disordered. Several bond lengths and angles in these chains deviate from normal values due to the averaging of disordered structures.

Table 1. Crystal data for **F8-4**, **F8-6**, **F8-7**, and **F8-11**.

	F8-4		**F8-6**	**F8-7**	**F8-11**
T [K]	200	100	200	200	130
formula		$C_{21}H_{17}F_{17}O_3$	$C_{23}H_{21}F_{17}O_3$	$C_{24}H_{23}F_{17}O_3$	$C_{28}H_{31}F_{17}O_3$
M_r		640.34	668.40	682.42	738.53
crystal shape	plate	plate	plate	plate	needle
crystal system	monoclinic	monoclinic	monoclinic	monoclinic	triclinic
space group	$P2_1/a$	$P2_1/n$	$P2_1$	$P2_1$	$P\bar{1}$
a [Å]	10.863(2)	26.348(2)	28.463(10)	29.821(5)	9.5272(11)
b [Å]	9.813(13)	9.5144(7)	9.030(2)	8.9051(11)	59.697(12)
c [Å]	23.900(5)	31.673(2)	5.1960(14)	5.1843(7)	5.434(2)
α [°]	90	90	90	90	90.50(3)
β [°]	91.302(6)	113.657(10)	91.84(3)	92.374(12)	92.40(2)
γ [°]	90	90	90	90	88.197(13)
V [Å³]	2496.2(9)	7272.8(9)	1334.7(7)	1375.6(3)	3086.3(14)
Z	4	12	2	2	4
ρ_{calcd} [g cm⁻³]	1.704	1.754	1.663	1.648	1.590

Results

Molecular structures: The crystal data and molecular structures of **F8-4**, **F8-6**, **F8-7** and **F8-11** are shown in Table 1 and Figure 2, respectively. There are three crystallographically independent molecules, A, B, and C, in **F8-4** (100 K) and two molecules, A and B, in **F8-11**. The molecular structures of **F8-4** are essentially the same at 100 K and 200 K except for the degree of disorder. At 100 K, the fluorine atoms of molecules B and especially C are still highly disordered.
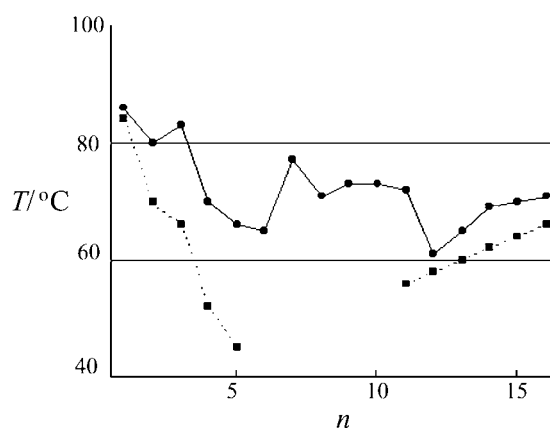
The C-C-C angles of ordered atoms in R_f chains are still slightly larger (113–118°) than usual, which suggests that the increase is caused by the presence of large fluorine atoms. The ethoxy skeleton, O3-C8-C9-C10, has a twisted conformation in all the cases, as shown in Table 2. Each R_f chain (C10–C17), except for the highly disordered **F8-4**(C), is slightly twisted in the same sense within a molecule and is attributed to F—F repulsion.[30] On the other hand, the R_h chains have an all-*trans* conformation except for **F8-4**.

In **F8-7**, the core moiety is disordered. The benzene ring (C1–C6), C7, and O3 are highly planar with root mean devi-
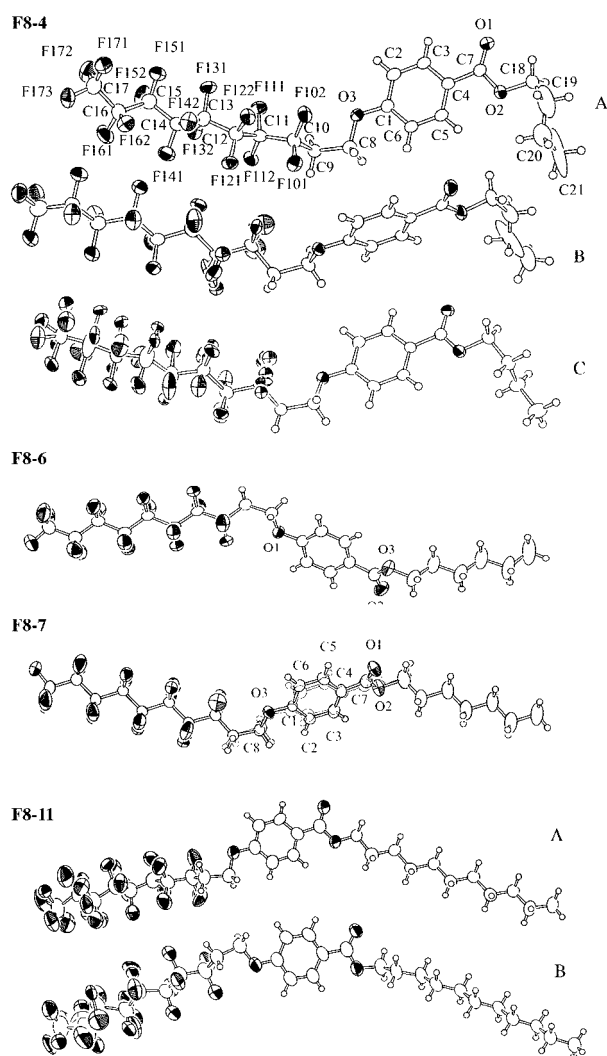
Figure 2. Molecular structures with the numbering scheme for non-hydrogen atoms of **F8-4** (100 K), **F8-6** (200 K), **F8-7** (200 K), and **F8-11** (130 K). Displacement ellipsoids are shown at the 50% probability level. All the molecules are numbered in similar ways. For **F8-7**, the disordered core moiety with minor occupancy is shown in gray.

ations of 0.012 and 0.05 Å for the major and minor conformers with occupation factors of 0.8 and 0.2, respectively. The dihedral angle between the two planes is 85.5(6)°, that is, almost perpendicular.

The molecules of **F8-4**, **F8-6**, and **F8-7** are Z-shaped, although those of **F8-6** and **F8-7** are much extended, while **F8-11** is bow-shaped (bent), as is **F8-2**.

Crystal packing: Figure 3 (top) shows the crystal structure of **F8-4** at 100 K viewed along the b axis. Crystallographically independent molecules, A, B, and C, are shown in purple, black, and green, respectively. The cell at 100 K is three times the size of that at 200 K, with the b axis common and $a' = a + 2c$ and $c' = -a + c$, whereby a and c are the axes of the high-temperature cell and a' and c' are those of the low-temperature one. The packing patterns are essentially the same at 200 K and 100 K. A crystal, that had previously been cooled to 130 K and then heated to room temperature, had the high-temperature cell, showing a reversible phase transition. The structure viewed along the [1 0 1] direction is shown in Figure 3 (lower part). Here, the nearest neighbors of respective molecules are shown separately for clarity. The butyl chain extends towards the R_f chain of a neighboring molecule, leading to the partial overlap of R_f chains.

The R_f and R_h chains of the middle members of the series (**F8-6** and **F8-7**) aggregate alternately (alternate type), as shown in Figure 4. Interatomic distances between the R_f and R_h chains are not shorter than the sum of the van der Waals radii of the fluorine and hydrogen atoms (1.47 and 1.20 Å, respectively[31]), showing that there are no special interactions such as C−H···F hydrogen bonds between the chains.

On the other hand, the R_f and R_h chains in **F8-11** aggregate separately (separate type), as shown in Figure 5. The core moieties and R_f chains are parallel to the b axis, while the R_h chains are tilted with respect to the axis (40°).

The schematic diagram of these structures (Figure 6) as well as that of **F8-2** shows a systematic structural change depending on the chain lengths; the separate-type structure for **F8-2** and **F8-11**, and the alternate-type structure for **F8-6** and **F8-7**. The structure of **F8-4** is similar to those of **F8-6** and **F8-7** in that adjacent molecules are arranged in opposite directions, as shown in Figure 3. However, the overlap of the R_f chains is more significant than in **F8-6** and **F8-7**, and so is regarded as an intermediate-type structure.

Computational studies: In molecular crystals, molecular and crystal structures are determined by intermolecular interactions. The intermolecular binding energy and geometries can be determined, in principle, by solving the Schrödinger equation for an assembly of

Table 2. Torsion angles of the R_f and R_h chains of **F8-4**, **F8-6**, **F8-7**, and **F8-11**.

| | F8-4 | | | F8-6 | F8-7 | F8-11 | |
	A	B	C			A	B
O3-C8-C9-C10	−81.6(5)	70.4(6)	68.4(5)	−71.2(5)	72.7(7)	77.5(10)	−66.1(12)
C8-C9-C10-C11	164.7(4)	175.1(5)	176.3(4)	−177.5(3)	171.9(5)	174.7(9)	−160.8(10)
C9-C10-C11-C12	164.8(4)	169.2(5)	177.6(6)	−176.6(4)	176.4(5)	175.2(10)	−172.3(11)
C10-C11-C12-C13	161.6(4)	168.7(5)	−179.4(7)	−175.8(4)	176.1(5)	162.9(10)	−169.3(11)
C11-C12-C13-C14	164.4(4)	165.3(5)	−179.7(11)	−171.5(3)	176.0(5)	171.5(10)	−168.8(14)
C12-C13-C14-C15	162.5(4)	167.0(5)	−171.9(19)	−173.5(4)	176.7(5)	168.1(11)	−175.5(13)
C13-C14-C15-C16	164.3(4)	170.6(4)	−169(3)	−173.8(4)	178.6(5)	171.5(11)	−171.9(14)
C14-C15-C16-C17	162.7(5)	175.9(5)	−160(4)	−178.6(5)	178.4(7)	174.7(12)	−163.8(15)
O2-C18-C19-C20	45.2(12)	−27(2)	−70.9(5)	−176.6(5)	177.2(7)	177.6(7)	166.7(8)
C18-C19-C20-C21	72.7(13)	−172.6(17)	179.3(5)	173.2(5)	−172.0(7)	176.3(7)	−169.4(8)
C19-C20-C21-C22				179.0(5)	−178.2(6)	−178.0(8)	175.6(7)
C20-C21-C22-C23				177.3(6)	−175.1(7)	177.9(8)	−175.1(7)
C21-C22-C23-C24					178.0(7)	179.6(8)	178.6(7)
C22-C23-C24-C25						178.1(8)	−179.9(7)
C23-C24-C25-C26						176.4(7)	178.4(7)
C24-C25-C26-C27						178.4(8)	−179.5(7)
C25-C26-C27-C28						178.5(8)	179.7(7)
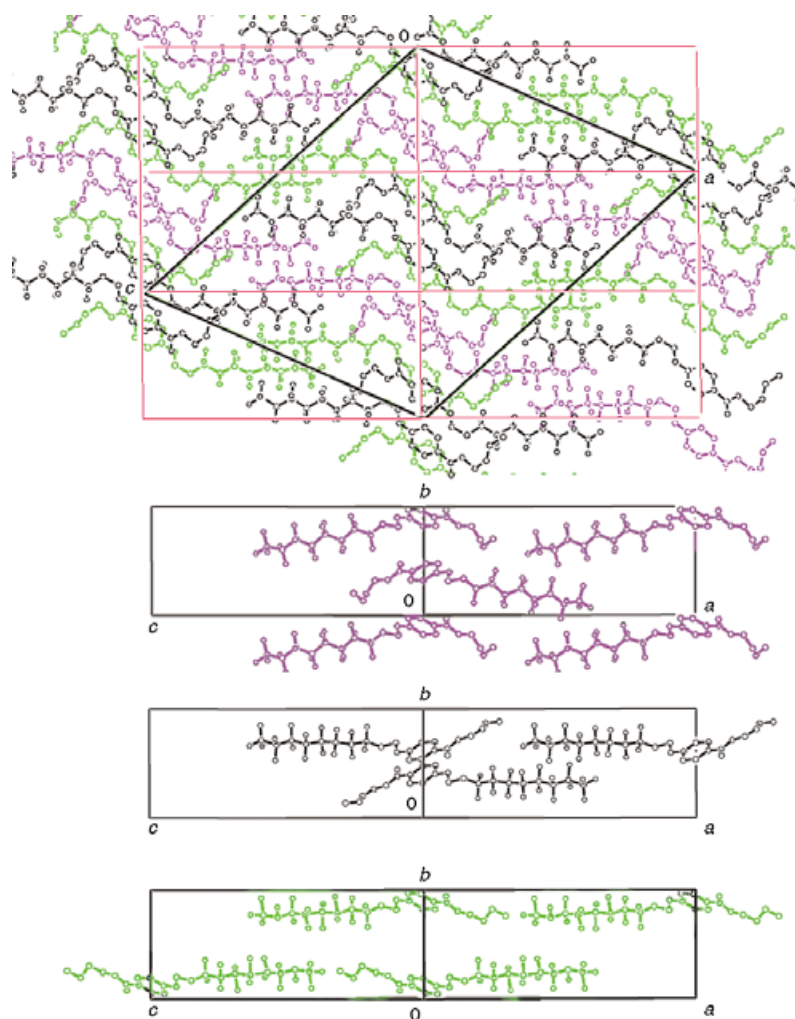
Figure 3. The crystal structure of **F8-4** at 100 K viewed along the *b* axis (top) and along the [101] diagonal (lower three). Hydrogen atoms and disordered atoms with minor occupancies are omitted for simplicity. Molecules A, B, and C are shown in purple, black, and green, respectively. Red lines denote the cell of the higher temperature phase in which all the molecules are equivalent. In the lower part of the figure, nearest neighbors are shown separately for respective molecules: molecules A related by 2_1 axes and molecules B and C related by inversion centers.

ate the intermolecular interactions by ab initio molecular orbital (MO) methods, it is necessary to employ highly sophisticated ab initio theory in the treatment of electron correlation effects and also a large number of basis functions. Such ab initio approaches may not be applicable to the large molecules treated here, simply because of the huge computational costs. The semiempirical MO method is an alternative approach. In this method, molecular integrals are evaluated approximately by using empirical parameters to reproduce the experimental data (geometries, heats of formation, dipole moments, and ionization potentials) of a set of molecules. Compared with ab initio methods, the computational costs are significantly reduced, but of course quantitative evaluations of intermolecular interactions can not be expected. Moreover, it is still practically impossible to treat a large number of molecules in a straightforward manner. In the present study, the semiempirical MO method, AM1, has been applied to estimate intermolecular interactions between four nearest molecules (tetramer) in crystals, in order to discuss, at least, the tendency of the interactions.
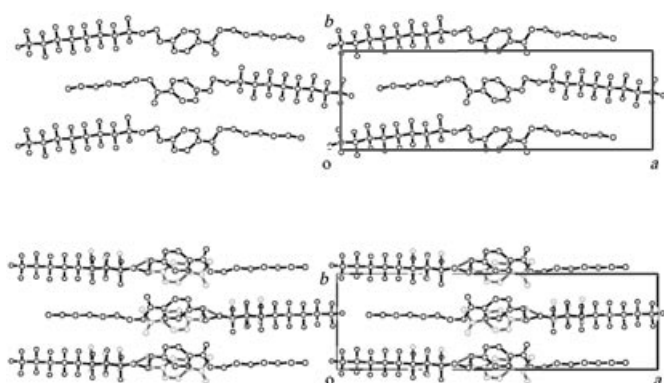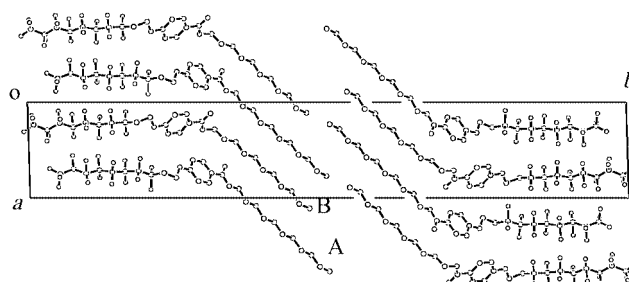

Figure 4. The crystal structure of **F8-6** (top) and **F8-7** (bottom). Hydrogen atoms are omitted for simplicity. For **F8-7**, the disordered moiety with minor occupancy is shown in gray.

Figure 5. The crystal structure of **F8-11**. Hydrogen atoms and disordered atoms with minor occupancies are omitted for simplicity.

molecules. It is difficult, however, to evaluate the intermolecular interactions accurately, because they are much weaker than intramolecular interactions. In order to evalu-

The molecular structures of the separate type (**F8-2** and **F8-11**) are different to those of the alternate type (**F8-6** and **F8-7**): bent and extended, respectively. The difference is caused by the 180° rotation of the ester linkages. The energy difference between the bent and extended molecules, calcu-
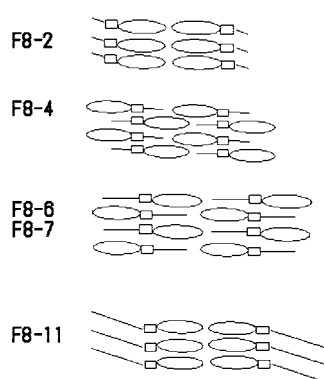
Figure 6. Schematic diagram of the crystal structures of **F8-2**, **F8-4**, **F8-6**, **F8-7** and **F8-11**. Ellipsoids, lines and squares denote R_f and R_h chains and the core moieties, respectively.

lated by using the AM1 method, is almost negligible for **F8-2** and **F8-6**: the bent molecule is more stable by $0.13 \, \text{kcal mol}^{-1}$ for the former with no energy difference between the molecules of the latter. Therefore, the molecular shapes are determined by the requirements of crystal packing.

We evaluated the intermolecular interactions in the tetramers of crystals of **F8-2** and **F8-11** (separate type), and **F8-6** (alternate type). The structures of the tetramers used in the calculations were as described in detail in the computational procedures section of the Experimental section. To determine the structure of each tetramer, geometry optimization was carried out, starting with the molecules in the respective crystal structures, as determined by X-ray analysis. Figure 7 shows the resultant fully optimized structures obtained with two different conditions, GNORM = 1.0 and GNORM = 5.0, whereby GNORM = x indicates that geometry optimization stops when the norm of the energy gradients for each atom of the tetramer becomes less than
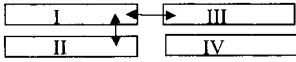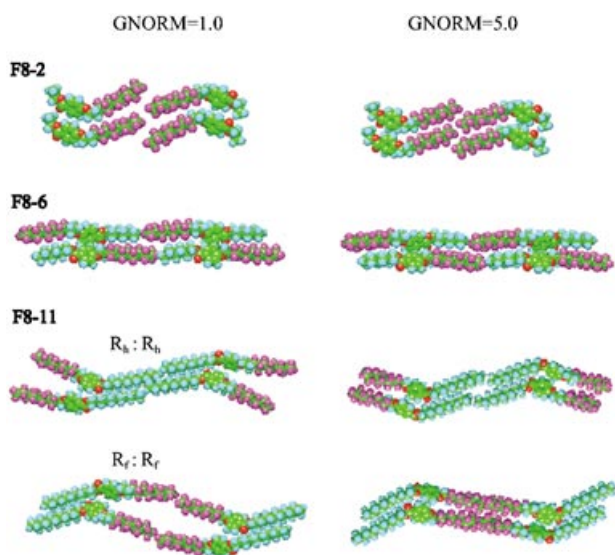

Figure 7. Optimized molecules with GNORM = 1 (left) and GNORM = 5 (right). The tetramer of **F8-11** shown here is of model 1. Fluorine and hydrogen atoms are shown in pink and blue, respectively.

$x \, \text{kcal mol}^{-1} \text{Å}^{-1}$. As shown in Figure 7, in the optimizations with GNORM = 1.0, the R_f chains separate in the separate type **F8-2** and **F8-11** molecules, while the R_f and R_h chains of the alternate type **F8-6** maintain chain contact. On the other hand, in the optimized structures obtained with GNORM = 5.0, intramolecular parameters were almost fully optimized, while the molecular conformations and intermolecular geometries were essentially maintained including the twisted moieties of the ethoxy groups. The following energy partition analyses were performed for the structures determined with GNORM = 5.0.

The intermolecular interaction (ΔE) of the tetramer is defined as the difference in the heat of formation of the tetramer and the sum of those of the four isolated monomers. Thus, the binding energy is defined as $-\Delta E$. In the calculations on the four isolated monomers, the geometrical structures of the respective monomers were taken from those in the tetramer optimized with GNORM = 5.0. The results are summarized in Table 3. The tetramers of **F8-2** and **F8-6** (real) were stabilized. For **F8-11**, the tetramer with the R_h chains inside is more stable than that with the R_f chains inside. For **F8-11** with R_f chains inside, models 1 and 2 show destabilization of the tetramer, while model 3 gives slight stabilization. The difference results from the geometry of the tetramer, especially the lateral overlap of the molecules, as discussed below.

In the AM1 method, the total energy can be divided into contributions from the respective atoms and atom pairs because of the neglect of the diatomic differential overlap (NDDO) approximation. The binding energy of the tetramer can also be partitioned into contributions from those within each monomer and from each pair of monomers. By taking a partial sum of the interatomic energy of atoms that belong to different monomers, we can discuss the origin of intermonomer interactions. First, interactions between molecular pairs, lateral (I–II) and longitudinal (I–III), were evaluated. As shown in Table 3, the contribution of the former is much larger. Note that interactions between parallel molecules in the separate type as well as antiparallel molecules in the alternate type are negative (attractive). Discrepancies between the total energy (ΔE) and the sum of the interactions between I–II and I–III are attributed to the fact that destabilization of monomers due to the change of electron density distribution between isolated and aggregated molecules was included in the calculation of ΔE, while only two-center intermonomer contributions were calculated for I–II and I–III interactions. Good correlation, however, exists between the two evaluations.

Next, contributions from the interactions between different moieties were evaluated. For this purpose, a molecule was divided into three fragments, that is, R_f, R_h and the remaining core moiety. The results for the interactions between I–II pairs are shown in Table 3. There are two different geometries for the R_f–core, R_f–R_h, and R_h–core pairs, respectively. Interactions between cores are positive for the separate type, and negative for the alternate type. It is reasonable that parallel cores are repulsive in the former, while antiparallel cores are attractive in the latter. Interactions between R_f chains are slightly positive with almost the same

Table 3. Results of the calculations [kcal mol^{-1}]. The results for the real alternate-type and hypothetical separate-type crystals of **F8-6**, derived from **F8-11**, are shown.

	Model[a]	Configuration[b]	ΔE[c]	I–II	I–III	Energy partition between I–II[c]					
						core–core	R_f–R_f	R_h–R_h	R_f–core	R_f–R_h	R_h–core
F8-2		R_f–R_f	−1.33	−3.26	0.24	2.74	0.64	2.72	0.16	−0.39	−4.96
									−1.74	−0.50	−1.94
F8-6 (real)			−2.22	−6.24	0.11	−6.53	0.12	1.22	0.47	−0.82	−0.02
									0.59	−2.12	0.83
F8-11	1	R_f–R_f	0.68	−3.37	0.16	2.88	0.88	0.36	0.14	−0.53	−5.10
									0.15	−0.33	−1.82
		R_h–R_h	−1.72	−6.06	0.06	2.81	0.65	−1.46	0.13	−0.53	−5.67
									0.25	−0.35	−1.80
	2	R_f–R_f	0.75	−2.56	0.21	2.27	0.94	−0.29	0.10	−0.42	−2.00
									−0.42	−0.37	−2.38
		R_h–R_h	−0.41	−2.51	−0.93	2.28	0.90	−0.18	0.13	−0.43	−2.06
									−0.42	−0.37	−2.37
	3	R_f–R_f	−0.62	−7.67	0.08	4.41	0.52	−2.84	−1.34	−0.52	−2.28
									0.21	−0.41	−5.42
		R_h–R_h	−1.02	−7.75	0.08	4.41	0.57	−2.93	−1.39	−0.54	−2.28
									0.20	−0.40	−5.40
F8-6 (hypothetical separate type)	1	R_f–R_f	−0.08	−2.91	0.17	2.96	0.64	2.76	0.62	−1.03	−6.29
									0.39	−0.56	−2.41
	2	R_f–R_f	1.84	−0.92	0.07	2.25	0.92	1.42	0.10	−0.45	−2.03
									−0.39	−0.36	−2.38
	3	R_f–R_f	−0.27	−4.62	0.14	4.35	0.46	0.50	−1.63	−0.53	−2.20
									0.19	−0.41	−5.36

[a] See Experimental section for details of models 1, 2, and 3. [b] R_f–R_f and R_h–R_h denote the arrangements with R_f and R_h chains inside, respectively. [c] For tetramer.

value in all cases except for **F8-6** (separate type), in which the R_f chains are far from each other. Repulsive interactions between the R_f chains are due to the head-to-head contacts of strong dipole moments in the C−F bonds of neighboring molecules. On the other hand, interactions between R_h chains depend largely on the chain length and the geometry of the tetramers. For **F8-11**, the larger the core-core repulsion is, the larger the R_h–R_h attraction is owing to the degree of lateral overlap of the corresponding moieties. For shorter members of the series, positive values were obtained, for which reasonable explanation could not be found. Probably, more aggregation would be necessary for the interaction to be attractive. On the other hand, interactions between R_f and R_h chains are always negative. Attractive interactions between R_f and R_h chains may be attributed to the induction effect of the strong dipole of a C−F bond on the C−H bond. In the alternate type **F8-6**, in which R_f and R_h chains are the nearest-neighbor moieties, these interactions are relatively large. In other cases, the R_f and R_h chains are far from each other, but still show attractive interactions. Similarly, cores and R_h chains are strongly attractive except for in **F8-6**. In contrast, interactions between cores and R_f chains are slightly repulsive in many cases.

Hypothetical separate-type structures of **F8-6**, derived from the molecular arrangements of **F8-11** by cutting off C_5H_{10} from the chains, were also examined. The trends in the binding energy and energy partition for models 1, 2, and 3 of **F8-6** coincide with those of **F8-11**. It is shown that the alternate type is more stable than any of the separate types, which agrees with experimental observation of the alternate

type. Moreover, the melting points of middle members of the series are higher than those extrapolated from shorter and longer members, as shown in Figure 1.

Discussion

Intermolecular interactions in crystals: As shown in Figure 6, crystal structures change systematically depending on the chain lengths: the separate type for shorter and longer members, and the alternate type for middle members. The bent molecules in the former case result from the requirements of close packing of significantly different cross sections of R_f and R_h chains. On the other hand, extended molecules with similar lengths of R_f and R_h chains fill the space efficiently in the alternate arrangement. However, a separate type is also geometrically possible for middle members, because both the shorter and longer members adopt this type of structure. If the tendency to micro-segregation was strong enough, the separate type would be realized also for the middle members. Moreover, **F8-4** has an intermediate type of overlapping of R_f chains. These facts suggest that micro-segregation is not always dominant. Similar situations have been encountered in several cases. Swallow-tailed compounds with R_f chains in the "tails" produce smectic phases with antiparallel arrangements of molecules, while those with an R_f chain in the "head" show columnar phases with segregation of R_f and R_h moieties.[32] Biphenyl compounds with R_f moieties in different positions in the chains show different smectic phases (S_A and S_E) with quite different mo-

lecular arrangements.[21b] Further, a pentaerythritol derivative with benzene rings bearing R_f and R_h chains side-by-side has a more stable columnar phase than the nonfluorinated counterpart.[12a] These facts are well understood in terms of the attractive interactions between R_f–R_h pairs, as described in the previous section.

The results of computational analysis show that the major contributions to the molecular aggregation to be core–core interactions in the case of the alternate type (**F8-6**) and core–R_h interactions in the case of the separate type (**F8-2** and **F8-11**). In **F8-11**, interactions between R_h chains become significant as the lateral molecular overlap becomes large. Interactions are slightly repulsive between R_f chains while they are attractive between R_f and R_h chains even when the chains are at a distance. Also the attractive interactions between the cores and R_h chains are larger than those between the cores and R_f chains.

In the limited model of four molecules, the contributions of the respective moieties have been evaluated: weakly repulsive interactions between R_f chains are shown. In the bulk state, molecules around the tetramer would affect the situation, especially dipole–dipole interactions, by working as dielectric media and/or by cancelling the different directional dipole–dipole interactions. However, it is expected that the relative contributions obtained here for the tetramers are still valid as a simple model.

Relationships between crystal and liquid crystal structures: In a previous study,[9b] the layer thickness (d) in the S_A phase was measured to be 30.0, 28.7, 28.5, and 27.9 Å for **F8-1**, **F8-2**, **F8-3**, and **F8-4**, respectively; this gives ratios of layer thickness to molecular length (l) of the extended shape of 1.36, 1.22, 1.12, and 1.08. Thus, it was concluded that the S_A phase of the shorter members is not a simple monolayer but an interdigitated one. For a similar mesogen, methyl perfluorooctylbutyloxybenzoate, d/l was determined to be 1.35 and a model with overlapping R_f chains was proposed, and was designated as bimolecular S_A.[8] On the other hand, d/l for **F8-12** was determined to be 1.72, which is much greater than one. Thus, for the S_A phase of **F8-12**, an interdigitated model with overlapping R_f chains in the middle part of a layer was proposed.[9b]

The crystal structures determined here do not transform directly to the S_A phase on heating. Nevertheless, they are expected to show characteristic features of molecular aggregation. Actually, their behavior is closely related to their liquid crystallinity: the shorter and longer members with the separate-type packing produce the S_A phase on cooling from the isotropic phase, while the middle members with the alternate-type packing do not. It is interpreted that in the latter systems, the tendency towards micro-segregation is not strong enough to maintain the S_A phase.

It is interesting that the ratio (d/l) decreases as the R_h chain length increases in the shorter members. A plausible explanation lies in the change of crystal structure from the bimolecular arrangement of the separate type (**F8-2**) to the partially overlapping arrangement of the intermediate type (**F8-4**): lateral intermolecular interactions and, hence, lateral molecular overlap increase as the R_h chain length increases.

Unfortunately the layer thickness of **F8-11** was not measured due to the instability of the supercooled S_A phase. However, the layer thickness (60 Å) of the S_A phase of **F8-12** is comparable to the dimension of the b axis of **F8-11** (59.697 Å). As two methylene groups in the bilayer contribute less than 3 Å (5%), another model is proposed for the molecular arrangement of the longer members in the S_A phase based on the crystal structure of **F8-11**. R_f and R_h chains are separated in a bilayer arrangement as in the crystal and melting R_h chains fill the space between layers of rather rigid R_f chains. It was concluded that the activation barrier for bond rotation is higher in the R_f chains than in the R_h chains.[33] The present model is consistent with an average distance between adjacent molecules of 5–6 Å due to the greater contribution of fluorine atoms than hydrogen atoms to the reflection intensity and also due to the higher degree of order in the R_f chains. This model also avoids the large gaps between R_h chains of the previous model. It is interpreted that the intermolecular interactions between R_h chains are strong enough for longer members to produce the bilayer structures, but not for shorter members.

Conclusions

First, systematic change of crystal structures depending on the chain length was found. Secondly, these structures are closely related to the mesophase behaviour. Thirdly, intermolecular interactions were estimated for tetramers, which indicated slightly repulsive interactions between R_f chains.

From these results, we conclude that the primary effect of fluorination is to give a molecule rigidity, which determines the molecular shape. To accommodate the rigid molecules in a crystal lattice as densely as possible, a separate type of packing is favorable in cases in which the lengths of R_f and R_h chains are very different, in contrast to the case of R_f and R_h chains of similar lengths. It is confirmed that the interactions between R_f chains are small compared with those between other moieties and that they are forced to aggregate due to the exclusion from other moieties. Thus, the effect is dependent on the geometries and intermolecular interactions of other moieties.

Experimental Section

The compounds were synthesized previously.[9] Single crystals were obtained by slow evaporation from a solution of dichloromethane and ethanol. Two different crystals were obtained for **F8-11**: thin plate and thin needle. The former, which was obtained at about 260 K, collapsed rapidly at room temperature.

X-ray crystal structure analysis: Experimental details of data collection and the final results of refinements are summarized in Table 4. Data were collected at low temperatures, because the data obtained at room temperature could hardly be solved due to the highly disordered fluorine atoms. Absorption correction was carried out based on a Ψ scan for **F8-6**, **F8-7** and **F8-11**. Structures were solved by applying SHELXS97[34] (**F8-11**) and SHELXS86[35] (others) and refined by applying SHELXL97[36] on $|F|^2$. Hydrogen atom positions were geometrically calculated and included in intensity calculations but were not refined.

Table 4. Experimental details of data collection and refinement.

	F8-4		F8-6	F8-7	F8-11
T [K]	200	100	200	200	130
crystal size [mm]	$0.3 \times 0.15 \times 0.1$		$0.4 \times 0.3 \times 0.05$	$0.4 \times 0.3 \times 0.05$	$0.1 \times 0.1 \times 0.2$
diffractometer	RAPID			AFC-7R	
X-ray source	Mo ($\lambda = 0.71069$ Å)			Cu ($\lambda = 1.54178$ Å)	
μ [mm^{-1}]	0.196	0.202	1.717	1.679	1.544
min/max transmission	0.969	0.949	0.643	0.817	0.916
$2\theta_{max}$ [°]	60	60	135	135	135
total reflns	29733	80102	6683	4349	10876
reflns used in refinement	7305	21073	4772	3384	9645
observed reflns [$I > 2\sigma(I)$]	2566	10196	4180	2631	3854
parameters	495	1289	389	465	947
independent reflns	7305	21073	2616	2635	9645
R(int)	0.046	0.053	0.085	0.049	0.058
R_1 (obsd reflns)	0.1653	0.1381	0.0706	0.0701	0.1248
wR_2 (obsd reflns)	0.4426	0.3501	0.1969	0.2268	0.3439
S	1.405	1.226	1.035	1.144	1.343
Δ/σ	0.464	0.500	0.018	0.431	0.104
$\Delta\rho$ [e Å^{-3}]	1.22/−0.57	2.09/−0.93	0.36/−0.28	0.56/−0.37	0.70/−0.57

For **F8-4**, the data obtained at 200 K on the AFC-7R diffractometer gave only a poor result. Data sets were collected again at 200 and 100 K on a RAPID diffractometer. The results obtained from the data, however, still gave large R values, as shown in Table 4. At 200 K, all the fluorine atoms were highly disordered: each atom was divided into two or three portions and yet the resultant temperature ellipsoids of anisotropically refined atoms were large and elongated. At 100 K, two of the three crystallographically independent molecules still had highly disordered R_f chains with several peaks of up to 2 e Å^{-3} around them.

For **F8-7**, the R_f chains were disordered at the inner moiety of the chain. Furthermore, when the refinement with anisotropic temperature ellipsoids for most non-hydrogen atoms converged to $R_1 = 0.103$, residual peaks around 1 e Å^{-3} appeared to form a definite structure of the core moiety composed of a benzene ring, an alkoxy O atom and an ester linkage. Assignment of these atoms as a disordered conformer with a small occupation factor of 0.2 led to $R_1 = 0.070$ without any significant distortion of the geometry. For **F8-11**, the relatively large R_1 and wR_2 values can be attributed to the highly disordered R_f chains and the low diffraction intensities due to the very thin crystal.

CCDC-220044–220047 (**F8-4** (100 K), **F8-6**, **F8-7**, and **F8-11**) contain the supplementary crystallographic data for this paper. These data can be obtained free of charge via www.ccdc.cam.ac.uk/conts/retrieving.html (or from the Cambridge Crystallographic Data Centre, 12 Union Road, Cambridge CB2 1EZ, UK (fax: (+44)1223-336-033; or e-mail: deposit@ccdc.cam.ac.uk).

Computational procedures: Semiempirical MO calculations were carried out on **F8-2**, **F8-6**, and **F8-11** by using the AM1 method in the MOPAC2000 software package.[29] As the target molecular system, the structures of the tetramers (four molecules closest to each other) were taken from the respective crystal structures determined by X-ray analysis. The tetramer of **F8-6** with alternate packing is uniquely chosen as the *ab* plane. For **F8-2**, there are two choices, the *ab* and *bc* planes, of which we took the latter with the larger lateral overlapping of molecules. For **F8-11**, there are more choices because of the two crystallographically independent molecules, A and B. In addition, tetramers with R_f chains inside and outside were examined because it was expected that the contributions from both R_f and R_h are significant and comparable. Six cases were examined in total: $[A(x,y,z)+B(x,y,z)+A(1−x,−y,1−z)+B(1−x,−y,1−z)]$ (model 1), $[A(x,y,z)+B(1+x,y,z)+A(2−x,−y,1−z)+B(1−x,−y,1−z)]$ (model 2), and $[A(x,y,z)+A(x,y,z+1)+B(1−x,−y,1−z)+B(1−x,−y,2−z)]$ (model 3) for the arrangements with R_f chains inside and $[A(x,y,z)+B(x,y,z)+A(1−x,1−y,2−z)+B(1−x,1−y,2−z)]$ (model 1), $[A(x,y,z)+B(1+x,y,z)+A(2−x,1−y,2−z)+B(1−x,1−y,2−z)]$ (model 2), and $[A(x,y,z)+A(x,y,z+1)+B(1−x,1−y,2−z)+B(1−x,1−y,3−z)]$ (model 3) for the arrangements with R_h chains inside. For simplicity, disordered structures were truncated to

the ideally ordered structures. Hypothetical separate-type structures of **F8-6** were derived from the molecular arrangements of **F8-11** by cutting off C_5H_{10} from the chains. In this case, only arrangements with R_f chains inside were obtained for the three models mentioned above. Geometry optimizations were performed with GNORM=5 for the respective tetramers with no symmetry restraints to avoid additional energy change. The binding energies were calculated for the resultant structures. The intermolecular interactions were analyzed by the energy partition (ENPART) option of MOPAC2000.

[1] P.-G. Lassahn, C. Tszchucke, W. Bannwarth, C. Janiak, *Z. Naturforsch. Teil B* **2003**, *58*, 1063–1068, and references therein.

[2] a) H. E. Katz, A. J. Lovinger, J. Johnson, C. Kloc, T. Siegrist, W. Li, Y.-Y. Lin, A. Dodabalapur, *Nature* **2000**, *404*, 478–481; b) H. E. Katz, J. Johnson, A. J. Lovinger, W. Li, *J. Am. Chem. Soc.* **2000**, *122*, 7787–7792; c) H. E. Katz, T. Siegrist, J. H. Schon, C. Kloc, B. Batlogg, A. J. Lovinger, J. Johnson, *ChemPhysChem* **2001**, *2*, 167–172.

[3] A. Facchetti, Y. Deng, A. Wang, Y. Koide, H. Sirringhaus, T. J. Marks, R. H. Friend, *Angew. Chem.* **2000**, *112*, 4721–4725; *Angew. Chem. Int. Ed.* **2000**, *39*, 4547–4551.

[4] For a review, see: F. Guittard, E. T. de Givenchy, S. Geribaldi, A. Cambon, *J. Fluorine Chem.* **1999**, *100*, 85–96.

[5] T. Doi, Y. Sakurai, A. Tamatani, S. Takenaka, S. Kusabayashi, Y. Nishihata, H. Teraushi, *J. Mater. Chem.* **1991**, *1*, 169–173.

[6] H. T. Nguyen, G. Sigaud, M. F. Archard, F. Hardouin, R. J. Twieg, K. Betterton, *Liq. Cryst.* **1991**, *10*, 389–396.

[7] S. Takenaka, *J. Chem. Soc. Chem. Commun.* **1992**, 1748–1749.

[8] G. Johansson, V. Percec, G. Ungar, K. Smith, *Chem. Mater.* **1997**, *9*, 164–175.

[9] a) H. Okamoto, H. Murai, S. Takenaka, *Bull. Chem. Soc. Jpn.* **1997**, *70*, 3163–3166; b) M. Duan, H. Okamoto, V. F. Petrov, S. Takenaka, *Bull. Chem. Soc. Jpn.* **1998**, *71*, 2735–2739.

[10] G. Fornasieri, F. Guittard, S. Geribaldi, *Liq. Cryst.* **2003**, *30*, 663–669.

[11] a) M. Prehm, S. Diele, M. K. Das, C. Tschierske, *J. Am. Chem. Soc.* **2003**, *125*, 614–615; b) X. Cheng, M. Prehm, M. K. Das, J. Kain, U. Baumeister, S. Diele, D. Leine, A. Blume, C. Tschierske, *J. Am. Chem. Soc.* **2003**, *125*, 10977–10996.

[12] a) A. Pegenau, X. H. Cheng, C. Tschierske, P. Göring, S. Diele, *New J. Chem.* **1999**, *23*, 465–467; b) X. H. Cheng, S. Diele, C. Tschierske, *Angew. Chem.* **2000**, *112*, 605–608; *Angew. Chem. Int. Ed.* **2000**, *39*, 592–595.

[13] a) V. Percec, G. Johansson, G. Ungar, J. Zhou, *J. Am. Chem. Soc.* **1996**, *118*, 9855–9866; b) S. D. Hudson, H.-T. Jung, V. Percec, W.-D. Cho, G. Johansson, G. Ungar, V. S. K. Balagurusamy, *Science* **1997**, *278*, 449–452.

[14] V. Percec, M. Glodde, T. K. Bera, Y. Miura, I. Shiyanovskaya, K. D. Singer, V. S. K. Balagurusamy, P. A. Heiney, I. Schnell, A. Rapp, H.-W. Spiess, S. D. Hudson, H. Duan, *Nature* **2002**, *419*, 384–387.

[15] V. Percec, M. Glodde, G. Johansson, V. S. K. Balagurusamy, P. A. Heiney, *Angew. Chem.* **2003**, *115*, 4474–4478; *Angew. Chem. Int. Ed.* **2003**, *42*, 4338–4342.

[16] a) C. Santaella, P. Vierling, J. G. Riess, *Angew. Chem.* **1991**, *103*, 584–586; *Angew. Chem. Int. Ed. Engl.* **1991**, *30*, 567–568; b) M.-P. Kraft, F. Giulieri, J. G. Riess, *Angew. Chem.* **1993**, *105*, 783–785; *Angew. Chem. Int. Ed. Engl.* **1993**, *32*, 741–743.

[17] A. Skoulios, D. Guillon, *Mol. Cryst. Liq. Cryst.* **1988**, *165*, 317–332.
[18] Y. Hendrikx, A. M. Levelut, *Mol. Cryst. Liq. Cryst.* **1988**, *165*, 233–263.
[19] C. Tschierske, *J. Mater. Chem.* **1998**, *8*, 1485–1508.
[20] W. Chen, B. Wunderlich, *Macromol. Chem. Phys.* **1999**, *200*, 283–311.
[21] a) F. Tournilhac, L. M. Blinov, J. Simon, S. V. Yablonsky, *Nature* **1992**, *359*, 621–623; b) S. Pensec, F.-G. Tournilhac, P. Bassoul, C. Durliat, *J. Phys. Chem. B* **1998**, *102*, 52–60.
[22] B. E. Smart in *Organofluorine Chemistry: Principles and Commercial Applications* (Eds.: R. E. Banks, B. E. Smart, J. C. Tatlow), Plenum, New York, **1994**, pp. 57–88.
[23] F. T. T. Huque, K. Jones, R. A. Saunders, J. A. Platts, *J. Fluorine Chem.* **2002**, *115*, 119–128.
[24] M. Skiba, M. Skiba-Lahiani, P. Arnaud, *J. Inclusion Phenom. Macrocyclic Chem.* **2002**, *44*, 151–154.
[25] P. Kromm, J.-P. Bideau, M. Cotrait, C. Destrade, H. Nguyen, *Acta Crystallogr. Sect. C* **1994**, *50*, 112–115.
[26] P. Kromm, H. Allouchi, J.-P. Bideau, M. Cotrait, H. T. Nguyen, *Acta Crystallogr. Sect. C* **1995**, *51*, 1229–1231.

[27] H. T. Nguyen, J. C. Rouillon, A. Babeau, J. P. Marcerou, G. Sigaud, M. Cotrait, H. Allouchi, *Liq. Cryst.* **1999**, *26*, 1007–1019.
[28] K. Hori, C. Kubo, H. Okamoto, S. Takenaka, *Mol. Cryst. Liq. Cryst.* **2001**, *365*, 617–625.
[29] MOPAC2000, version 1.0, Fujitsu, Tokyo (Japan), **1999**.
[30] C. W. Bunn, E. R. Howells, *Nature* **1954**, *174*, 549–551.
[31] A. Bondi, *J. Phys. Chem.* **1964**, *68*, 441–451.
[32] D. Lose, S. Diele, G. Pelzl, E. Dietzmann, W. Weissflog, *Liq. Cryst.* **1998**, *24*, 707–717.
[33] D. F. Eaton, B. E. Smart, *J. Am. Chem. Soc.* **1990**, *112*, 2821–2823.
[34] G. M. Sheldrick, SHELXS97. Program for the Solution of Crystal Structures, University of Göttingen (Germany), **1997**.
[35] G. M. Sheldrick, SHELXS86. Program for the Solution of Crystal Structures, University of Göttingen (Germany), **1986**.
[36] G. M. Sheldrick, SHELXL97. Program for the Refinement of Crystal Structures, University of Göttingen (Germany), **1997**.